JOURNAL OF GEOPHYSICAL RESEARCH, VOL. , NO. , PAGES 1–14,

Implementation of Noah land-surface model advances in the National Centers for Environmental Prediction operational mesoscale Eta model

M. B. Ek,[1] K. E. Mitchell,[1] Y. Lin,[1] E. Rogers,[1] P. Grunmann,[1] V. Koren,[2] G. Gayno,[3] and J. D. Tarpley,[4]

Abstract. We present the impact tests that proceeded the most recent operational upgrades to the land-surface model used in the National Centers for Environmental Prediction (NCEP) mesoscale Eta model whose operational domain includes North America. These improvements consist of changes to the 'Noah' land-surface model (LSM) physics, most notable in the area of cold season processes. Results indicate improved performance in forecasting low-level temperature and humidity, with improvements to (or without affecting) the overall performance of the Eta model quantitative precipitation scores and upper-air verification statistics. Remaining issues that directly affect the Noah LSM performance in the Eta model include physical parameterizations of radiation and clouds which affect the amount of available energy at the surface, and stable boundary layer and surface layer processes which affect surface turbulent heat fluxes and ultimately the surface energy budget.

1. Introduction

During the past two decades, a number of advances in land-surface models (LSMs) have been made in simulating surface energy and water fluxes and the surface energy and water budgets in response to near-surface atmospheric forcing. The companion evolution of soil moisture, soil temperature, and snowpack are important to the surface energy and water budgets on short-term (e.g. daily) to long-term (e.g. seasonal to annual) time scales, and they in turn depend on surface conditions (such as vegetation state and soil texture). Increasingly then, the parameterizations of land-surface processes have become more physically based due to heightened multi-disciplinary cooperation and increased knowledge in the fields of meteorology, hydrology, and plant and soil physics.

Surface fluxes provide the necessary lower boundary conditions for numerical weather prediction (NWP) and climate models. These weather and climate models are computationally intensive and as such the LSMs utilized must be efficient in their representation of land-surface processes. At the onset of the 1990s, the National Centers for Environmental Prediction (NCEP) started testing the efficient LSM developed for use in NWP at Oregon State University (OSU) beginning in the middle 1980s (Mahrt and Pan 1984; Pan and Mahrt 1987). The original OSU LSM consisted of two soil layers with thermal conduction equations for soil temperature and a form of Richardson's equation for soil moisture. The effect of stomatal control by plants was represented via a constant 'plant coefficient' (fractional, 0 to 1) to account for atmospheric influences, multiplied by the soil moisture availability (fractional, 0 to 1) to account for the soil moisture influence, finally multiplied by the potential evaporation (Mahrt and Ek 1984). Later, a variable plant coefficient which accounted for stomatal control was related to a canopy conductance formulation using the common 'big leaf' approach (Jarvis 1976; Noilhan and Planton 1989), reported in Holtslag and Ek (1996), where canopy conductance is modeled as a function of soil moisture availability and atmospheric conditions (solar insolation, temperature, and humidity).

During the 1990s, NCEP greatly expanded its land-surface modeling collaborations via several components of the Global Energy and Water Cycle Experiment (GEWEX), most notably, the GEWEX Continental-scale International Project (GCIP) and the Project for Intercomparison of Land-surface Parameterization Schemes (PILPS). These collaborations included the Office of Hydrological Development (OHD) of the National Weather Service, NESDIS, NASA, NCAR, the U.S. Air Force, and OSU and other university partners. As an outgrowth of these collaborations and their broad scope of LSM testing in both uncoupled and coupled mode over a wide range of space and time scales (see citations below), NCEP substantially enhanced the OSU LSM, now renamed the Noah LSM in recognition of the broad partnership above.

The mesoscale model forecast suite at NCEP is the Eta model (Janjić 1990, 1994, Black 1994, Mesinger 2000) and its

[1]National Centers for Environmental Prediction, Environmental Modeling Center (NCEP/EMC), 5200 Auth Road, Room 207, Suitland, Maryland 20746 USA. michael.ek@noaa.gov
[2]National Weather Service, Office of Hydrologic Development, Silver Spring, MD 20910
[3]HQ Air Force Weather Agency (AFWA), Offutt A.F.B., NE 68113
[4]NESDIS/ORA, 5200 Auth Road, Suitland, Maryland 20746 USA.

Paper number .
0148-0227/03/$9.00

Eta Data Assimilation System (EDAS, Rogers et al 1996), now run operationally at 12-km resolution with 60 layers. NCEP generally first implements the Noah LSM enhancements in the Eta-EDAS suite, followed later by implementation in the NCEP Global Forecast System (GFS). Before introducing the latest Noah LSM enhancements and tests that are the subject of this paper, we first briefly review the highlights of the earlier Noah LSM upgrades that have taken place in the Eta-EDAS suite at NCEP over the past seven years. These included an increase from two to four soil layers, modifications to the canopy conductance formulation (Chen et al 1996), bare soil evaporation and vegetation phenology (Betts et al 1997), surface runoff and infiltration (Schaake et al 1996), and thermal roughness length treatment in the surface layer exchange coefficients (F. Chen et al 1997). A key companion advance was the implementation of fully continuous self-cycling of soil moisture and temperature in the EDAS (without soil moisture nudging) in June 1998. Since then the Eta model initial soil moisture and temperature are sole products of the EDAS (namely the coupled Noah-Eta model and the land surface forcing internal to the EDAS) without undue drift in soil moisture and temperatures.

The above forerunner Noah LSM advances have yielded improved model performance, both in an offline mode (that is, atmospheric-forced LSM-only runs for specific sites or in two-dimensional horizontal land-surface domains), as well as coupled in the fully three-dimensional operational mesoscale Eta analysis and forecast system. Offline testing of the Noah LSM has involved several PILPS and related or similar projects (e.g. Chen et al 1996, T. H. Chen et al 1997, Qu et al 1998, Wood et al 1998, Chen and Mitchell 1999, Koren et al 1999, Schlosser et al 2000, Slater et al 2001, Boone et al 2001, Bowling et al 2001). Coupled evaluation has addressed performance of the Noah LSM in an NWP setting with focus on land-surface processes from local to continental scales (e.g. Berbery et al 1996, 1999, 2003, F. Chen et al 1997, Betts et al 1997, Yucel et al 1998, Hinkelman et al 1999, Angevine and Mitchell 2001, Berbery 2001, Marshall et al 2003).

Given the significant role GCIP has played in supporting land-surface model development at NCEP, it is appropriate to review the Noah LSM in this special GCIP issue. In describing the various model advances and when they occurred (see Table 1), this paper reviews upgrades to the physical parameterizations and land-surface fields used in and by the Noah LSM along with the companion impact tests in the coupled Noah/Eta-EDAS suite, for the cold season (section 2) and the warm season (section 5). This latest phase of Noah LSM advances described here embodies a 'generational' Noah LSM upgrade including the addition of frozen soil physics and major advances in snowpack-related physics (Koren et al 1999), significant improvements to bare soil evaporation, soil heat flux enhancements for bare soil, snow-covered and vegetated conditions, and some modest changes to canopy conductance. These Noah LSM upgrades address Eta model forecast biases in near-surface air temperature and relative humidity thought to be due in part to deficiencies in Noah LSM physics evident in uncoupled testing (described above).

This paper presents the follow-on testing to confirm in coupled mode the improvement anticipated from our uncoupled (offline) testing. The model testing and assessment includes regional verification of realtime parallel executions in winter, early spring, and summer, as well as individual case studies (under conditions of minimal large-scale forcing) in order to demonstrate model bias reductions. The most recent Noah LSM upgrades were tested in the NCEP mesoscale Eta model and then implemented in the Eta-EDAS suite operationally in July 2001, with an additional change in February 2002. We summarize our findings and suggest further Noah LSM improvements and future direction in section 4.

2. Cold season processes

Cold season processes are important in the evolution of the land-surface for a large fraction of the earth during many cold season months. In the presence of snow cover, albedo increases, surface roughness is often reduced, and the exchange of heat and moisture between land-surface and atmosphere is diminished, while sub-surface freezing reduces the movement of heat and moisture within the soil. All of these processes affect the surface energy budget and thus the surface fluxes, so it is necessary to include these effects in LSMs used in weather and climate models. These processes are included in the Noah LSM upgrades demonstrated herein, as well as other land-surface models (e.g. Viterbo et al 1999, Smirnova et al 2000, Boone et al 2000, Boone and Etchevers 2001). The improvements to the Noah LSM in the area of cold season processes were first made and tested in an offline mode by Koren et al (1999) and during the PILPS 2d exercise (Schlosser et al 2000, Slater et al 2001), and then in a coupled mode within the NCEP mesoscale Eta model as presented here.

2.1. Patchy snow cover and frozen soil

The cold season processes that have been added or improved are described in Koren et al (1999), and include the effect of latent heat release during soil water freezing in winter which ameliorates the typical underestimation (when frozen soil processes are ignored) of soil temperature (and thus surface and air temperatures) during soil freezing periods, and overestimation of temperatures during thawing periods. The frozen soil moisture content depends on the soil temperature, volumetric soil moisture, and characteristics dependent on soil texture. Additionally, a treatment of patchy (fractional) snow cover is introduced, which allows the surface temperature to exceed freezing. The previous formulation in the Noah LSM used all incoming energy to melt and sublimate the snowpack (which was considered uniform across a gridbox) until complete ablation. This bounded the surface skin temperature at $0^{\circ}C$ (in the solution of the single surface energy budget), resulting in the daytime low-level air temperature holding near freezing. The new Noah LSM formulation allows for patchy snow cover if the snow depth is below some threshold, and hence allows exposed ground, a lower albedo, more energy absorption, and the aggregate (gridbox) surface skin temperature (still corresponding to a single surface energy budget) to rise above 0°C. As such the surface sensible heat flux increases with a corresponding increase in low-level air temperature. The subgrid patchiness is related to the depth of the snow

Table 1. Timeline of Noah land-surface model (LSM) evolution, with references to relevant model physics and/or land-surface fields implemented in the NCEP operational mesoscale Eta model.

date	description	reference(s)
	Original OSU LSM (prior to NCEP era)	
	potential evaporation	Mahrt and Ek (1984)
	surface fluxes, soil hydraulics,	Mahrt and Pan (1984),
	and soil thermodynamics	and Pan and Mahrt (1987)
Noah LSM implementation in Eta model at NCEP (*assessed in an Eta model study)		
31 Jan 96	OSU LSM introduced into Eta model	Chen et al (1996)
	(GFS initial soil moisture & temperature)	
	surface runoff and infiltration	Schaake et al (1996)
24 Jul 96	ISLSCP vegetation greenness changes	
18 Feb 97	NESDIS vegetation greenness	Gutman & Ignatov (1998)
	bare soil evaporation changes	Betts et al (1997)*
	snow melt changes	Betts et al (1997)*
	thermal roughness length changes	F. Chen et al (1997)*
09 Feb 98	increase from 2 to 4 soil layers	
03 Jun 98	self-cycling Eta-EDAS soil moisture & temp.	
	NESDIS daily snow cover & sea ice analysis	Ramsay (1998)
Noah LSM upgrades (with assessment in Eta model) described in this study		
21 Jul 01	frozen soil physics	Koren et al (1999)
	snowpack physics upgrade	Koren et al (1999)
	maximum snow albedo climatology	Robinson and Kukla (1985)
	shallow snow thermal conductivity	Lunardini (1981)
	bare soil evaporation refinement	
	bare soil thermal conductivity changes	Peters-Lidard et al (1998)
	vegetation-reduced soil thermal conductivity	Peters-Lidard et al (1997)
	transpiration refinements	
26 Feb 02	patchy shallow snow thermal conductivity	

and surface characteristics, e.g. for a 'smoother' surface such as a grassland, a smaller snow depth threshold is required for 100% snow cover compared to a forest (Figure 1).

Moreover, the evolution of the snowpack density is added as a new snowpack state, and is governed via a time-dependent snow compaction algorithm, which includes the effect of new snowfall. Previously the snow depth was assumed to have a 'typical' 5:1 ratio, usually too low for new snowfall, but perhaps too high for an older snowpack. The snow density then affects the thermal conductivity through snow (previously assumed to be constant), which is important in determining the exchange of heat between the land-surface and atmosphere. Also, in the presence of frozen soil moisture, the moisture infiltration (i.e. of snowmelt water and precipitation) is reduced. These parameterizations have been adopted in the current version of the Noah LSM with some modifications, e.g. the computational efficiency of snow density formulation and frozen soil numerics have been greatly improved.

Below, we describe our further extensions to the Noah LSM in terms of cold season processes beyond those presented in Koren et al (1999).

2.2. Soil heat flux under snow

As the snowpack becomes very thin, it is difficult to estimate the large near-surface temperature gradients in the snow and upper soil layer, which sometimes leads to unrealistic spikes in the modeled values of the soil heat flux (G) through the snow and upper soil layer (e.g. as seen in Hinkelman et al 1999). The original formulation for G in the Noah LSM assumed a constant value for the snow thermal conductivity (0.35 W m^{-1} K^{-1}) with heat flux through the soil and snow determined as

$$G = K_s(T_s - T_{s1})/\Delta Z_s \quad (1)$$

where K_s is the snow thermal conductivity, T_s and T_{s1} are the surface (snow) skin and upper soil layer (mid-point) temperatures, respectively (with the restriction that $T_s \leq 273.15$), and ΔZ_s is the snow depth, assumed to be $10 \times SWE$, where SWE is the snow water equivalent (so a snow density ratio of 10:1). The solution for G was then bounded by ± 100 W m^{-2} for numerical stability because with a vanishing snowpack ($\Delta Z_s \rightarrow 0$), G could spike with large positive or negative values, depending on the gradient of $T_s - T_{s1}$ (Figure 2).

Therefore, the soil heat flux formulation in the Noah LSM has been modified to include the effect of heat flow through thin patchy snow cover. This is done by considering the thermal conductivity of a snowpack-plus-upper-soil-layer following a method described in Lunardini (1981), where heat flow can be in parallel, in series, or intermediate between the two. Here parallel heat flow through the snowpack-plus-upper-soil-layer is assumed which yields a larger thermal conductivity (than say, series), implicitly accounting for the non-uniform nature of snowpack cover. The effective thermal conductivity for the surface is then determined via a linear weighting between the snow-covered and non-snow-covered fractions (of a model gridbox), where

$$K_T = \Delta Z_s K_s + \Delta Z_{s1} K_{s1} \quad (2)$$

$$K_{eff} = \sigma_s K_T + (1 - \sigma_s) K_{s1} \quad (3)$$

where K_{s1}, K_T, K_{eff} are the thermal conductivities of the upper soil layer, snow-plus-upper-soil-layer, and patchy snow-covered surface (Figure 3), respectively, ΔZ_{s1} is the upper soil layer depth, and σ_s is the snow cover fraction ($0 \leq \sigma_s \leq 1$). The soil heat flux through the patchy snow-covered surface is then formulated as

$$G = \frac{K_{eff}(T_s - T_{s1})}{\Delta Z_s + \Delta Z_{s1}} \quad (4)$$

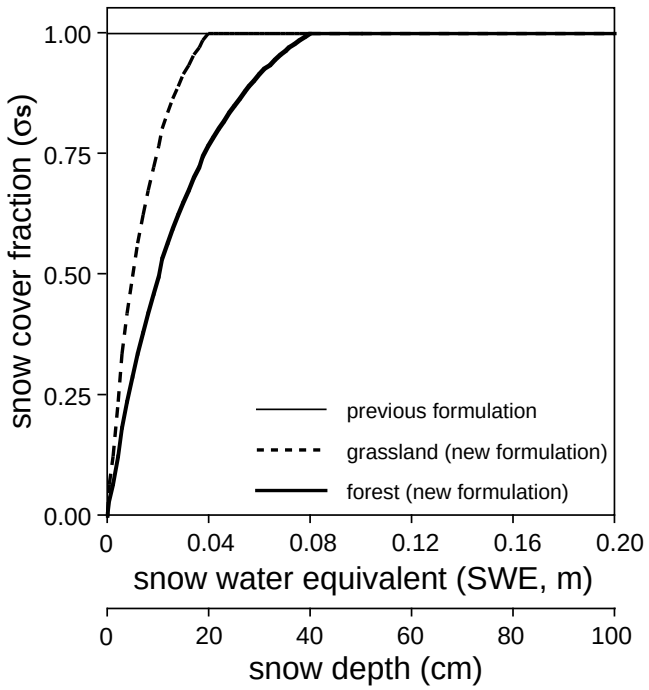

Figure 1. Snow cover fraction (σ_s) as a function of snow water equivalent (SWE, and snow depth assuming a snow density ratio of 5:1) for the previous Noah LSM formulation (thin line, $\sigma_s = 0$ for $SWE = 0$, and $\sigma_s = 1$ for $SWE > 0$), and for the new Noah LSM formulation for forest (thick solid line) and grassland (thick dashed line) vegetation classes.

In this formulation the thermal conductivity remains robustly defined even in the extremes of vanishing snow cover ($\Delta Z_s = 0, \sigma_s = 0, K_{eff} = K_{s1}$), or for a very deep snowpack ($\Delta Z_s \gg \Delta Z_{s1}$, $\sigma_s = 1$, $K_{eff} \rightarrow K_s$), which is quite important for numerical stability. Chang et al (1999) describe a similar thermal conductivity formulation (derived independently) adopted in another version of the OSU LSM which accounts for a vanishing snowpack depth, although they did not account for patchy snow cover (equivalent to setting $K_{eff} = K_T$). Patchy snow cover must be accounted for since it increases the heat flux between the surface and atmosphere (especially at smaller snow cover fractions) because of the typically larger thermal conductivity of soil compared to snow.

2.3. Albedo over snow

In the presence of snow cover, the surface albedo may be markedly increased due to the high albedo of snow (depending on vegetation cover). However, in conditions of shallow snowpack when snow first accumulates at the start of snowfall or diminishes due to snow sublimation or snow melt, there will be non snow-covered patchy areas, e.g. in a model gridbox. To account for this patchiness effect we formulate the surface albedo as a composite of a snow-covered and non-snow-covered surface as

$$\alpha = \alpha_0 + (1 - \sigma_f)\sigma_s(\alpha_s - \alpha_0) \quad (5)$$

where α, α_0, and α_s are the actual, snow-free, and maximum snow surface albedo, respectively, σ_f is the green vegetation fraction ($0 \leq \sigma_f \leq 1$), and σ_s is the snow cover fraction (defined earlier), as illustrated in Figure 4. As snow depth becomes zero, the albedo becomes the snow-free albedo ($\alpha = \alpha_0$). When the snow depth exceeds a threshold value (dependent on land-surface classification, e.g. vegetation type), snow cover is complete ($\sigma_s = 1$) and $\alpha = \alpha_s$, the maximum snow albedo (described below).

Over deep snow, the albedo of the surface is higher and in LSMs is often set to some uniformly large value, e.g. 0.55 previously in the Eta model. However, this can vary greatly depending on the surface character. For example, a conifer forest may have a lower albedo due to darker treetops sticking through a brighter (deep) snowpack, compared with a higher albedo for a completely snow-covered grassland. However, rather than use a maximum snow albedo simply as a function of the vegetation class or surface type (e.g. as in the ECMWF land-surface model, van den Hurk et al 2000), we use an annual maximum snow albedo climatology data set which extends the work of Robinson and Kukla (1985). Their original data set covered the area north of 25°N at 1° × 1° resolution, so for each 1° × 1° cell, the maximum snow albedo implicitly includes the effect of variable vegetation density (subgrid variability) within the same vegetation class. Note the differences between the North American boreal forests with lower maximum snow albedos due to more shading of the snowpack under the canopy, compared to the Great Plains grasslands with higher maximum snow albedos due to more open ground and exposed snow cover (Figure 5).

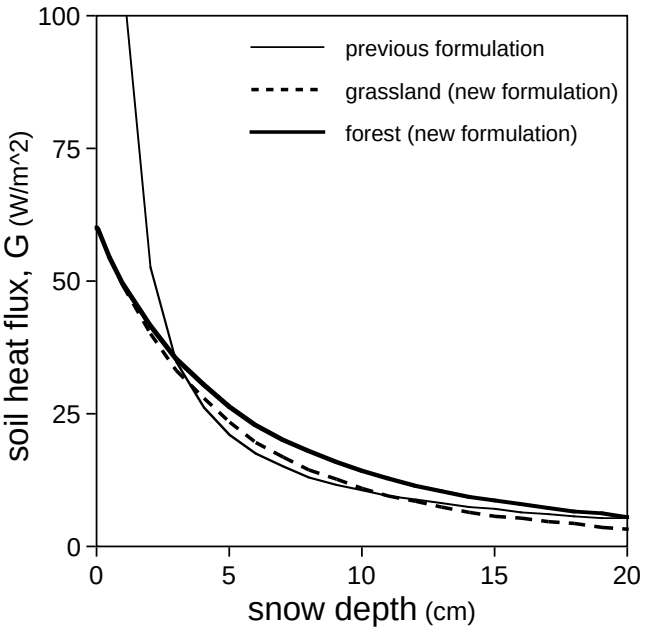

Figure 2. Soil heat flux (G) through patchy snow cover as a function of snow depth for the previous Noah LSM formulation (thin line), and the new Noah LSM formulation for forest (thick solid line) and grassland (thick dashed line) vegetation classes. Here we have assumed a temperature gradient of 3°K (old formulation: Eq. 1; new formulation: Eq. 4), and for the new formulation an upper soil layer volumetric soil moisture content of 0.29 (yields soil thermal conductivity of 1.0 W m^{-1} K^{-1} for Noah LSM soil texture class No. 2, silty clay loam) and snow density ratio of 5:1 (yields snow thermal conductivity of 0.108 W m^{-1} K^{-1}).

To populate a global 1° × 1° data base, the maximum snow albedos from the original data base were correlated with the SiB vegetation class (Dorman and Sellers 1989) over this region to determine any pattern by 'binning' the maximum snow albedo for a given vegetation class, then averaging and noting ranges. Indeed, the analysis showed a lower maximum snow albedo over forests than over short vegetation (i.e. grasslands, tundra). The average maximum snow albedo for a given vegetation class was then applied to the region south of 25°N, hence the more homogeneous 'look' of the data base in this 'filled' region. Since there were no maximum snow albedo values for the tropical forest regions in the original data base, the maximum snow albedo for this vegetation type was nominally set to the Matthews (1983) snow-free albedo for the vegetation type in these regions.

2.4. Snowpack initialization

Before showing model impact studies, we review how the snowpck is initialized in the Eta model since snow cover and snow depth are important initial conditions for LSMs during winter months in many regions. Previously, only the daily 47-km U.S. Air Force snow depth and sea-ice analysis was used in initializing snow and sea-ice in Eta model forecasts. While not an upgrade in the context of the study here, a 23-km northern hemisphere snow and ice chart (Figure 6) prepared operationally on a daily basis year-round by the Satellite Analysis Branch of the Satellite Services Division of NESDIS (Ramsay 1998) is being used operationally for the Noah LSM in the Eta-EDAS forecast system. This product provides superior information on the areal coverage of the snow and ice using visible imagery of the polar and geostationary (GOES) orbiting satellites as the primary tools for the analysis of this snow and ice cover, and relies on the human-interactive scrutiny of a trained satellite imagery analyst. Low-resolution visible data are used, augmented whenever possible by the visible high-resolution imagery and visible GOES, GMS, and METEOSAT data. In addition, ground weather observations and various DMSP microwave products are incorporated into this daily snow and ice chart.

The Eta model initialization interpolates the most recent 47-km U.S. Air Force (USAF) global snow depth analysis (Kopp and Kiess 1996) and the NESDIS snow cover analysis to create an initial snow cover and (actual) snow depth

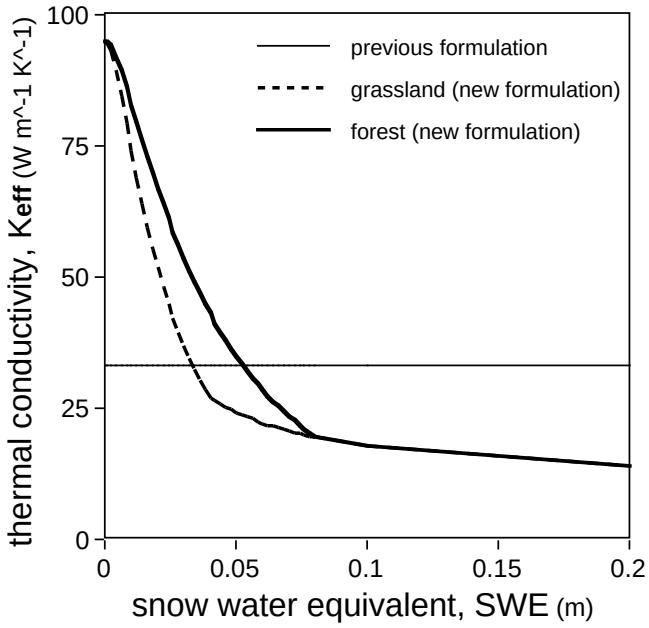

Figure 3. Thermal conductivity (K_{eff}) through patchy snow cover versus snow water equivalent (SWE) for the previous Noah LSM formulation (thin line, $K_{eff} = K_s$ = constant = 0.35 W m^{-1} K^{-1}), and new Noah LSM formulation for forest (thick solid line) and grassland (thick dashed line) vegetation classes, with the same patchiness corresponding to Figure 1, and soil and snow conditions as in Figure 2.

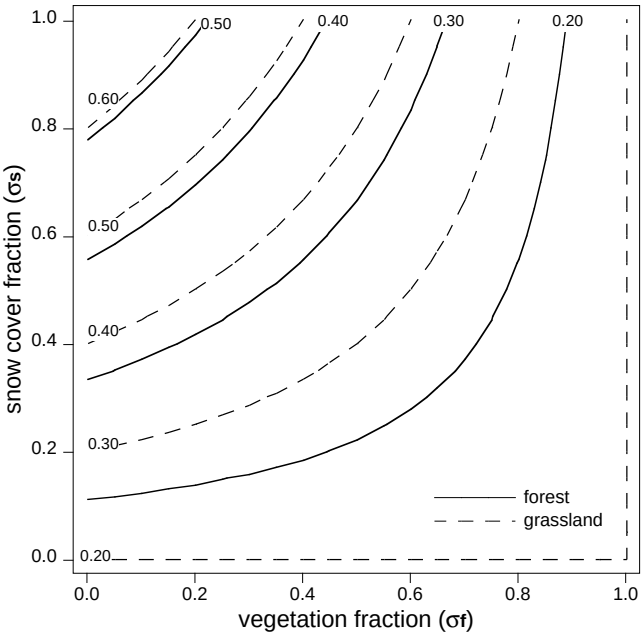

Figure 4. Surface albedo contours as a function of snow cover fraction versus green vegetation fraction with 'typical' forest (grassland) values for snow-free albedo, α_0=0.15 (α_0 = 0.20) and maximum snow albedo, α_s = 0.60 (α_s = 0.70).

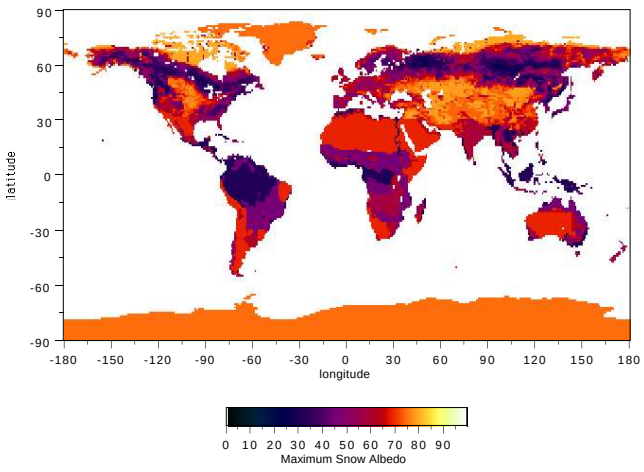

Figure 5. Maximum snow albedo based on Robinson and Kukla (1985).

analysis for use by the Noah LSM e.g. in Eta model runs. Snow water equivalent (SWE) is determined from the snow depth assuming a snow density ratio of 5:1. The NESDIS snow cover analysis is used as a quality control for the USAF snow depth analysis, i.e. if NESDIS indicates snow cover, the USAF snow depth is used, unless the USAF analysis indicates no snow depth in which case a minimal value is assigned to the model gridbox (2.5 cm snow depth, which yields 0.5 cm SWE); if NESDIS indicates no snow cover, this is assumed to be the case and any USAF snow depth is ignored.

2.5. Results from late winter snow-melt case

To assess the performance of the various modifications made to the Noah LSM in a coupled mode, we make several sets of model runs using the NCEP mesoscale Eta analysis and forecast system, that is, model runs made each day for both the 00Z and 12Z cycles, run out beyond 48 hours. These sets consist of Eta model runs made over a period of several weeks to over a month for different times of the year with the results then compared to the operational (control) runs and observations. Additionally, a number of events episodic in nature (case studies) are examined during the periods described above where model output is compared with observations for specific forecast cycles using individual station time series and (horizontal) geographical plots showing Eta model performance.

Under conditions of southerly warm advection over a daytime melting shallow snowpack, surface skin temperature was held at $0°C$ in the previous formulation in the Noah LSM, resulting in the 2-m air temperature holding near freezing, a condition noted by many NWS field offices and others. In the new Noah LSM formulation with patchy snow cover (section 2.1), the surface skin temperature may rise above 0°C, allowing the daytime 2-m air temperature to rise further above freezing. This is the case for 2 February 2001 at North Platte, Nebraska in the central US where the forecast 2-m air temperature is closer to the observed using the new Noah LSM formulation (Figure 7). So less energy goes towards melting the shallow snowpack (it lasts longer), and more energy goes towards surface sensible heating resulting in warmer 2-m air temperatures and hence a substantial reduction in the daytime cold bias. This also shows up in the closer agreement between forecast and observed mid-day 2-m air temperatures across this region of shallow melting snowpack (not shown).

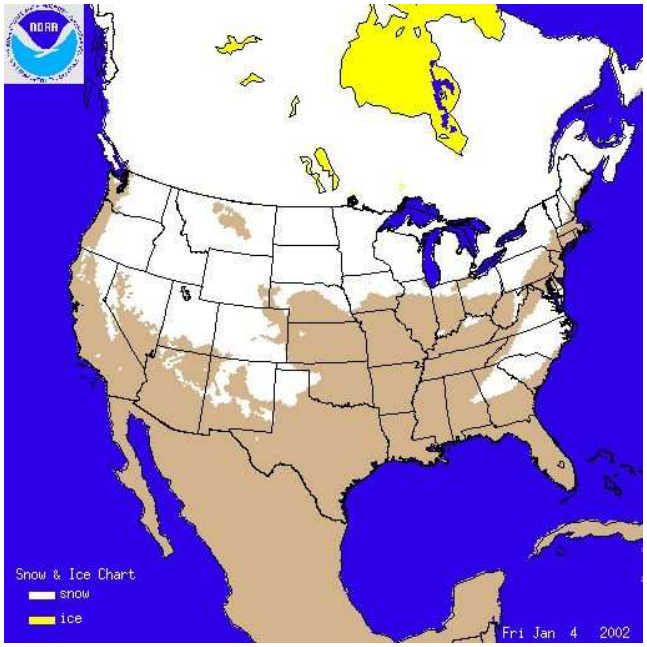

Figure 6. Snow cover over North America based on NESDIS snow cover analysis for 04 January 2002.

In order to assess model performance for longer periods (i.e. monthly) on a regional basis, we utilize the NCEP forecast verification system which provides statistics on near-surface verification of 2-meter air temperature and relative humidity from the operational and test versions of the Eta model. These statistics are generated for 22 different regions covering the Eta model domain, e.g. continental US and Alaska, and include monthly diurnal time series composites of the 00-hour through 48-hour forecast compared with observations. Monthly compositing allows smoothing of the transient nature of day-to-day variability in weather, so that patterns emerge which help evaluate and understand the diurnal nature of model forecasts related to the Noah LSM. As such, we can see a reduced cold bias with the new Noah LSM reflected in the composite plot of the diurnal cycles of the 2-m air temperature from the Eta model forecasts for the month of February 2001 in the eastern US (Figure 8), a

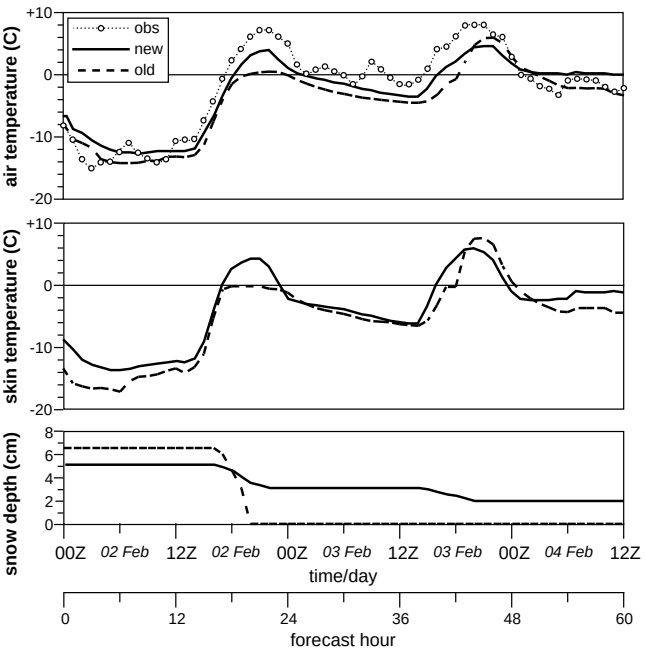

Figure 7. Observed (circles-dotted line) versus modeled 2-m air temperature (upper), surface skin temperature (middle), and snow depth (lower) for original (dashed lines) and new (solid lines) Noah LSM formulation for snow cover, at North Platte, Nebraska (60-hour Eta model forecast from 00Z 02 February 2001). The slight difference in the initial snow depths in the original versus new model reflects the different snowpack evolutions during the prior 24-hr model assimilation and analysis period.

region more likely to have patchy snow cover conditions.

2.6. Results from mid-winter nighttime cold bias case

During early January 2002 a snow event occurred in the southern Appalachian mountains from northeastern Georgia, through South Carolina, and into North Carolina and Virginia (Figure 6). Prompted by reports from NWS field offices, Eta model output was examined and showed a overly-strong temperature drop with a severe cold bias (5-10°C) in near-surface Eta model temperatures across this region after the appearance of snow cover. Using the modified thermal conductivity through the soil and snowpack which accounts for patchy snow cover (section 2.2), this results in more 'communication' with the warmer soil below. This gives greater soil heat flux from below at night, partly offsetting the strong nighttime radiative cooling over the new snow cover, resulting in warmer nighttime temperatures (Figure 9). The reduced nighttime cold bias with the new Noah LSM is reflected in the composite plot of the diurnal cycles of the 2-m air temperature from the Eta model forecasts for a month-long period during January through February 2002 in the western US (Figure 10), a region with more persistent snowpack. The remaining cold bias may be due to too little downward sensible heat flux in the stable boundary layer; underforecast low-level cloud cover and the associated downward longwave radiation may also play a role.

3. Warm season processes

While snowpack processes (e.g. snow sublimation) often dominate surface fluxes during the cold season, during the warm season a key component in the surface moisture flux is evapotranspiration via bare soil evaporation and plant transpiration. In the Noah LSM, evapotranspiration is modeled as the sum of transpiration from the plant canopy, direct ('bare soil') evaporation of soil water from the uppermost soil layer, and direct evaporation of canopy-intercepted water. These quantities come from an evaluation of a single surface energy budget for a given model gridbox. For complete details on plant transpiration and canopy conductance, and canopy evaporation, see Chen et al (1996, their section 3.1.2). The updated bare soil evaporation formulation is discussed in more detail in the next section.

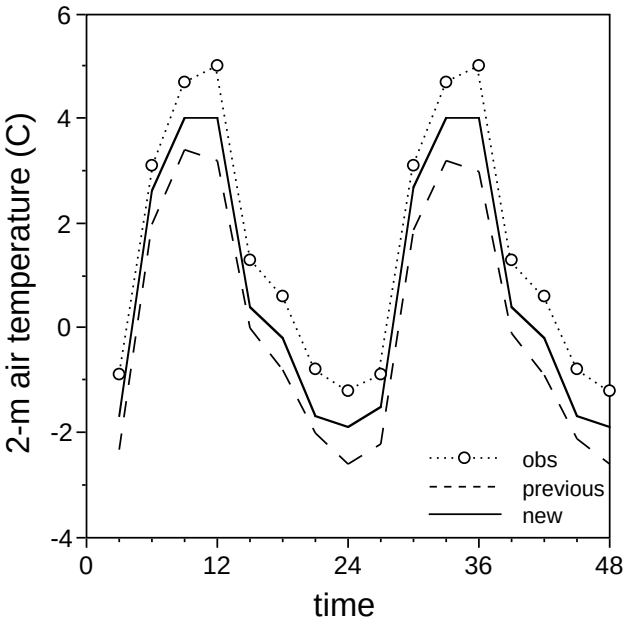

Figure 8. February 2001 monthly composite of 2-m air temperature, observations (circles-dotted line), and previous (dashed line) and new (solid line) Noah LSM for the eastern US (Eta 12Z cycle).

3.1. Bare soil evaporation

Direct soil evaporation (E_{dir}) is moisture flux from the non-vegetated (that is, the non-green portion, or 'bare soil' for shorthand) fraction of a model gridbox ($1 - \sigma_f$), and originally followed an explicit soil diffusivity formulation for moisture transport at the (bare soil) surface (Mahrt and Pan 1984). However, modeling experience showed that this formulation results in evaporation that falls off too rapidly as soil moisiture declines (reported in Betts et al 1997); a better alternative is formulated as

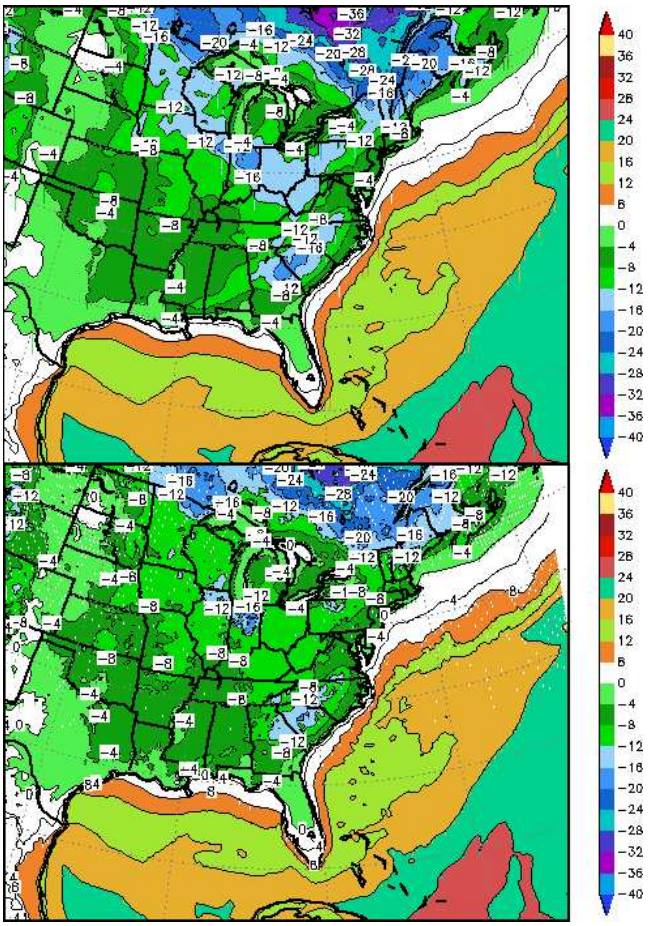

Figure 9. Eta model nighttime 2-meter air temperature with control (top) and new (bottom) soil heat flux formulation for patchy snow cover (36-hour forecast valid 12Z 04 January 2002). Note the region from northeast Georgia through southcentral Virginia, and along the 'snowline' in the US upper midwest and upper Ohio Valley as seen in Figure 6.

$$FX = (\Theta_1 - \Theta_{dry})/(\Theta_{sat} - \Theta_{dry}) \quad (6)$$

$$E_{dir} = (1 - \sigma_f)(FX)^{fx} E_p \quad (7)$$

where FX is the fraction of soil moisture saturation in the upper soil layer, Θ_1, Θ_{dry}, and Θ_{sat} are the soil moisture in the upper soil layer, air dry (minimum), and the saturation (porosity) values, respectively, and fx is an empirical coefficient. Nominally, $fx = 1$ yielding a linear function (i.e. Betts et al 1997, following Mahfouf and Noilhan 1991), though we have now modified it to be a non-linear function in order to more properly account for the large gradients in soil moisture near the surface. So with $fx = 2$, bare soil evaporation falls off more rapidly (in a quadratic manner) as the near-surface soil dries. This non-linear function then compensates for using the soil moisture content at the typically moister mid-point level of the upper soil layer where FX is evaluated, rather than the more appropriate (and most often drier) soil moisture content at the surface. This then more properly reflects the real process whereby as bare soil dries, the top few millimeters of the soil become significantly drier than the several centimeters below and thus act as a capping evaporative "crust" barrier at the upper boundary of the topmost soil layer.

3.2. Soil thermal conductivity changes

The soil thermal conductivity, including that of the upper soil layer (K_{s1}) used in the calculation of soil heat flux, is a function of soil texture and increases with increasing soil moisture content (Eq. 4, with $\Delta Z_s = 0$ and $K_{eff} = K_{s1}$). The nonlinear formulation by Al Nakshabandi and Khonke (1965, described in McCumber and Pielke 1981) has been commonly used in land-surface modeling for calculating thermal conductivity, but a less non-linear function following Johansen (1975) has been adopted for use in the Noah LSM (Figure 11). The advantage of Johansen (1975) is described in detail in Peters-Lidard et al (1998), and when compared to Al Nakshabandi and Khonke, the Johansen formulation appropriately yields more (*less*) thermal conductivity for drier (*moister*) soils, and thus greater (*lesser*) soil heat flux, which in turn leads to a more damped (*amplified*) diurnal signal in the surface skin and near-surface (e.g. 2-m) air temperatures.

In the presence of a vegetation layer, soil heat flux is reduced because of lowered heat conductivity through vegetation. This effect of vegetation may be accounted for explicitly, such as by using the leaf area index (LAI) as in BATS (Yang et al 1999), or implicitly, such as using a fixed thermal conductivity 'coefficient' dependent on surface classification (e.g., sparse vegetation, forest, etc. as in the ECMWF land-surface model; van den Hurk et al 2000). We adapt the explicit approach applied by Peters-Lidard et al (1997) wherein the soil thermal conductivity under vegetation (K_{veg}) is reduced from the 'bare soil' value (K_{s1}) by an exponential function of LAI. Here we adopt a similar alternate formulation using the vegetation fraction (σ_f) instead, where

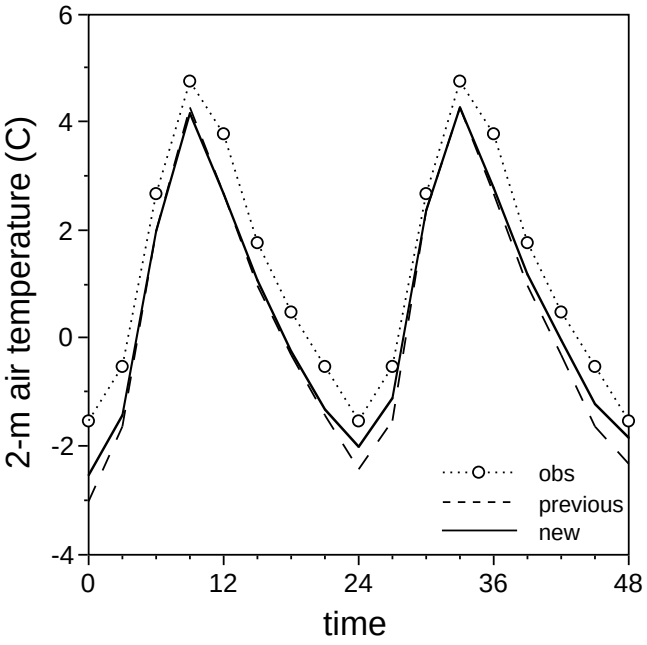

Figure 10. Monthly composite (during January through February 2002) of 2-m air temperature, observations (circles-dotted line), and previous (dashed line) and new (solid line) Noah LSM for the western US (Eta 12Z cycle).

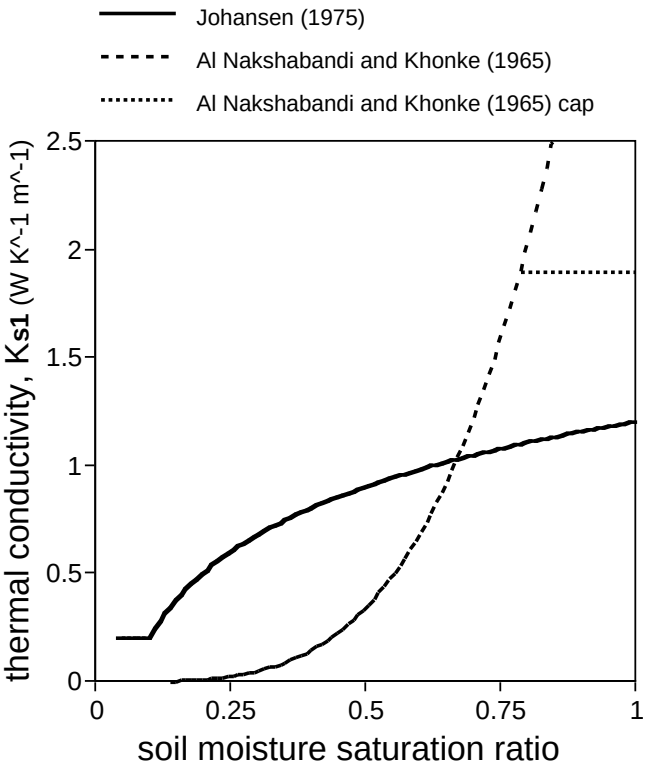

Figure 11. Soil thermal conductivity (K_{s1}) as a function of fractional soil moisture saturation, for the previous Noah LSM formulation following Al Nakshabandi and Khonke (1965, dashed line) versus the new formulation following Johansen (1975, solid line) for silty clay loam (Noah LSM soil texture class No. 2). The horizontal dotted line (at K_{s1}=1.9 W m^{-1} K^{-1}) represents an earlier attempt to limit (cap) the larger thermal conductivity values via Al Nakshabandi and Khonke at higher soil moisture conditions.

$$K_{veg} = K_{s1} exp(-\beta_{veg}\sigma_f), \quad (8)$$

where β_{veg} is an empirical coefficient, nominally equal to 2.0 following tests with the offline Noah LSM (Figure 12). So K_{veg} then replaces K_{s1} in the soil heat flux calculation (again, Eq. 4, with $\Delta Z_s = 0$ and $K_{eff} = K_{veg}$). We use σ_f to account for the seasonal changes in vegetation rather than LAI (see section 3.3).

3.3. Transpiration refinements

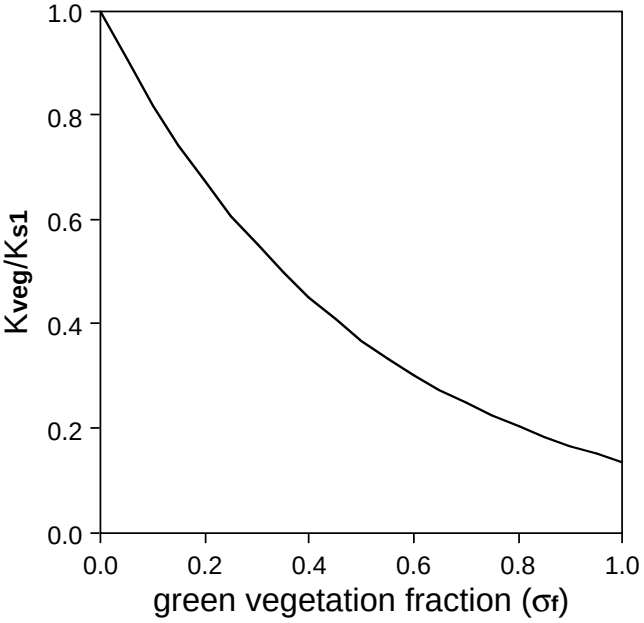

Figure 12. Ratio of soil thermal conductivity under vegetation to 'bare soil' soil thermal conductivity (K_{veg}/K_{s1}) as a function of green vegetation fraction.

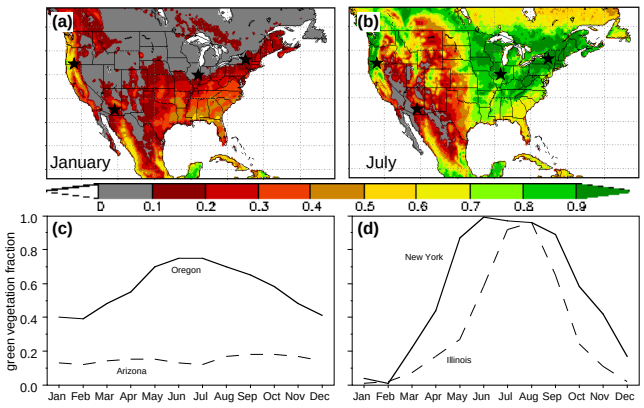

Figure 13. Green vegetation fraction based on NESDIS NDVI-based 15-km five-year climatology data set for the US in (a) January and (b) June, and annual cycle of green vegetation fraction near (c) Medford, Oregon (42.2°N,122.6°W) and Tucson, Arizona (32.2°N,111.0°W), and (d) Ithaca, New York (43.0°N,75.1°W) and Champaign, Illinois (40.0°N,88.4°W).

Plant transpiration can provide a dominant source of surface moisture flux especially in regions with large vegetation coverage during the warm season, using energy that might otherwise heat the surface. As such the explicit effects of vegetation have been incorporated into many LSMs used in NWP models, including the Noah LSM. Given a good physical parameterization for plant transpiration, land-surface models still require information on the vegetation class, and spatial coverage and seasonal greenness phenology of this vegetation for proper representation of the surface fluxes. Previously the ISLSCP 1°×1° monthly green vegetation data set was used (Sellers et al 1995), however experience showed that this data set had a low bias in greenness resulting in a low evaporation bias (Betts et al 1997). While not an upgrade in the context of the study here (as with the snow cover and depth analysis described in section 2.4), the monthly NESDIS NDVI-based 15-km five-year climatology data set (Gutman and Ignatov 1998) is being used operationally for the Noah LSM in the Eta-EDAS, providing monthly-varying green vegetation fraction for each model gridbox (Figure 13).

The Noah LSM uses the spatially and temporally varying green vegetation fraction (σ_f) to represent the seasonality of vegetation (described above), and treats the vegetation density through the leaf area index (LAI) as a constant for reasons outlined in Gutman and Ignatov (1998). Essentially, in creating their green vegetation fraction data set, Gutman and Ignatov (1998) had limited degrees of freedom, such that for a monthly-varying σ_f, LAI had to be fixed with a value on the order of $1-6$. This is not entirely surprising since as the greenness fraction within a particular gridbox increases, the LAI under that area (σ_f) does not vary as markedly. Though a modest change, due to a noted underprediction of

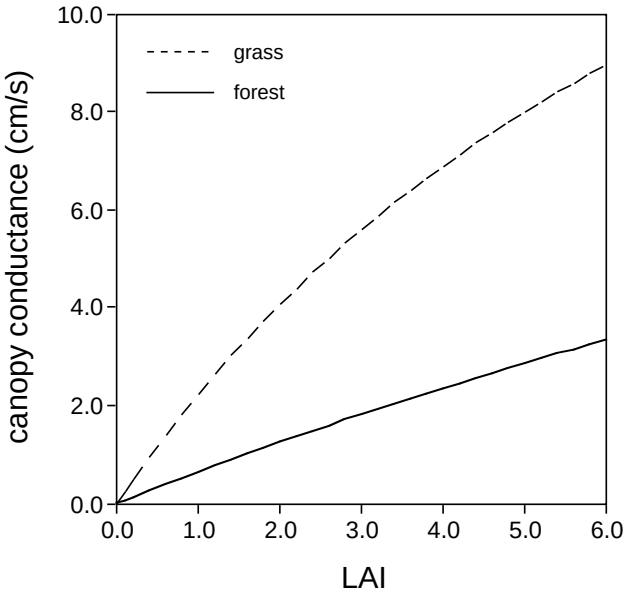

Figure 14. Canopy conductance as a function of LAI for forest (solid line) and grassland (dashed line) vegetation classes, with incoming solar radiation of 800 W m^{-2}, and non-limiting (no reduction of canopy conductance) effects of air temperature, atmospheric vapor pressure deficit and soil moisture availability.

transpiration in the Noah LSM, we increase the LAI from 1 to 4, which increases the canopy conductance (Figure 14), and thus increases transpiration and decreases surface sensible heat flux.

Additionally, we change the number of root layers (out of 4 total soil layers in the Noah LSM) for a particular vegetation class to more properly reflect the depth of root penetration, and thus the ability to extract water for transpiration. Previously the number of root layers was fixed (at 3) for all vegetation classes, but is now increased for forests (to 4), though reduced for tundra (to 2). Additionally, the 'glacial' vegetation class uses the same rooting depth as tundra since any vegetation greenness in a glacial region is assumed to be due to tundra.

3.4. Results from early spring case with sparsely vegetated, wet soil

Over wet soils with sparse green vegetation common during early spring, bare soil evaporation dominates the surface moisture flux; soil heat flux is more directly coupled with the atmosphere (due to less green vegetation cover) so the thermal conductivity for bare soil is more important. Under such conditions, previous Eta model testing showed that low-level humidity and temperature were too moist and cool, which resulted in a dampened diurnal temperature cycle due to excess bare soil evaporation, and excess soil heat flux because of too much heat going into (*coming out of*) the soil during daytime (*nighttime*).

This deficiency lead to the introduction of more optimal formulations for bare soil evaporation and soil thermal conductivity in the Noah LSM (sections 3.1 and 3.2). Now there is less bare soil evaporation due to a more nonlinear decrease in evaporation as wet soils dry slightly, and less soil heat flux due to reduced thermal conductivity in moist soils. We see that during spring 2001 parallel Eta model testing, in the upper mid-west with wet soils and sparse vegetation coverage during this time of year (annual cover that has not yet gone through 'green-up'), the previous (*new*) Noah LSM formulation yields higher (*lower*) near-surface dewpoints in the US upper midwest (Figure 15). With reduced surface evaporation and decreased soil heat flux (into the soil) under wet soil conditions, the low-level (e.g. 2-m) air temperature (*dew point*) is warmer (*lower*) and compares more favorably with observations (Figure 16). The reduced moist bias with the new Noah LSM is also reflected in the composite plot of the diurnal cycles of the relative humidity from the Eta model forecasts for the month of April 2001 in the US northern midwest region (Figure 17).

In the opposite conditions of dry soil moisture, Marshall (1998) and Marshall et al (2003) show that the new Noah LSM soil thermal conductivity formulation yields more soil heat flux for dry soils (re: section 3.2) during Oklahoma summertime such that an amplified diurnal temperature cycle is reduced, and is closer to the observations.

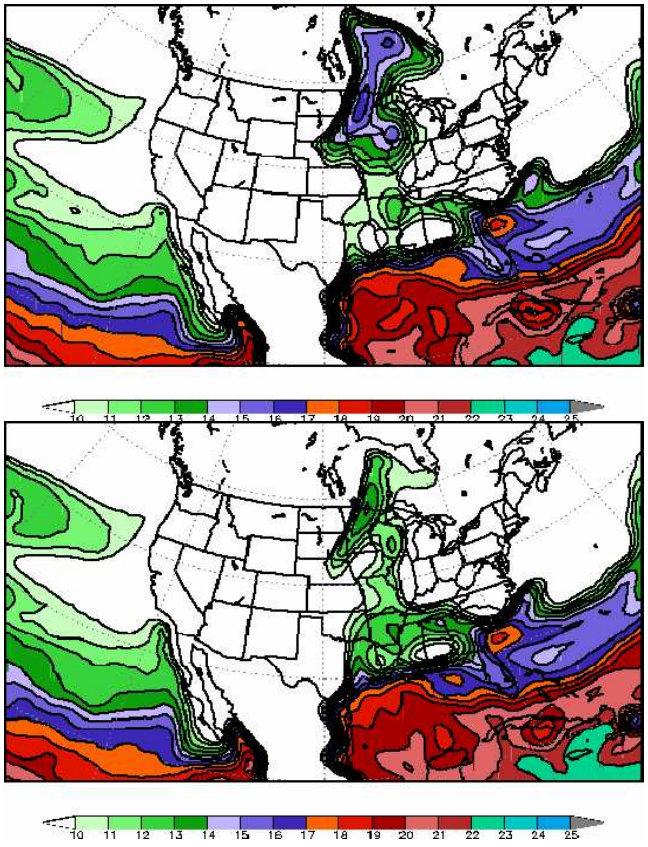

Figure 15. Dew point temperatures for the lowest 30 mb layer (nominally 300 m) above the surface with the old (top) and new Noah LSM (bottom) (60-hour Eta model forecast valid 00Z 30 April 2001). Note the reduced region of high dew point temperatures using the new Noah LSM over the sparsely vegetated wet soil regions in the US upper midwest and into south-central Canada at this time of year.

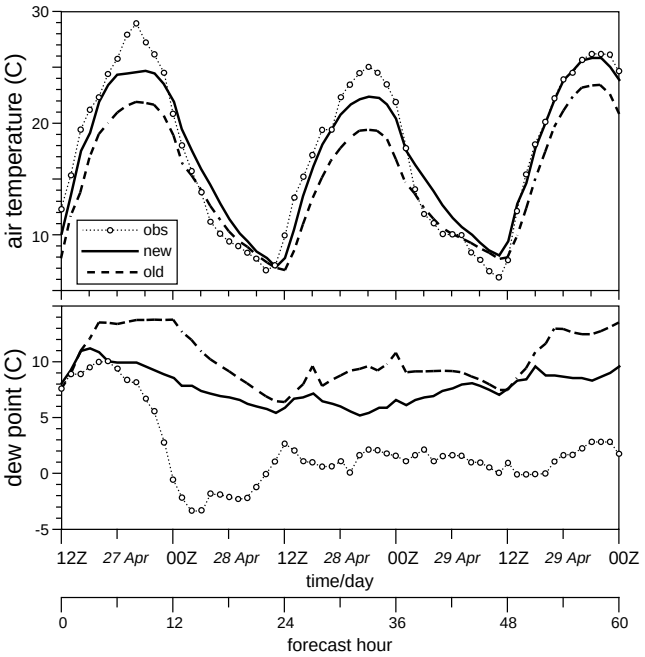

Figure 16. Observed (circles-dotted line) versus modeled 2-m air temperature (upper) and 2-m dew point (lower) for old (dashed lines) and new (solid lines) Noah LSM formulation, at Champaign, Ill. (60-hour Eta model forecast from 12Z 27 April 2001).

3.5. Results from mid-summer case with large green vegetation fraction

During summer months with large green vegetation fractions, plant transpiration dominates the surface moisture flux; soil heat flux is less directly coupled with the atmosphere (due to more green vegetation cover) so the effect of vegetation on soil thermal conductivity is important. A warm bias in the Eta model is noted in these regions because the Noah LSM produces a canopy conductance that is too low so transpiration is underpredicted, giving more available energy to surface heating (and thus temperatures), which can carry over into the nighttime and next day. This bias is addressed (modestly) via an increase in LAI in the new Noah LSM (section 3.3). This increases the canopy conductance and thus surface moisture flux, reducing sensible heat flux and decreasing the bias in low-level (e.g. 2-m) air temperature (Figure 18). We also note a small reduction in the warm bias with the new Noah LSM in the composite plot of the diurnal cycles of the air temperature from the Eta model forecasts for a month-long period during August and September 2000 in the US northern midwest region (Figure 19).

4. Summary and future direction

Various upgrades to the Noah land-surface model (LSM) have been made to address different biases in the NCEP mesoscale Eta model. We described analyses of various operational and retrospective runs of the Eta model using previous and upgraded versions of the Noah LSM. These analyses included individual case studies, as well as regional monthly composite plots of the diurnal cycles of observations versus Eta model output which helped us evaluate and understand the diurnal nature of model forecasts related to the Noah LSM.

From these the following conclusions may be drawn:

Upgrading snowpack and adding frozen soil physics are crucial in representing wintertime conditions. The previous cold biases in the wintertime low-level temperatures have been partially mitigated by including patchy snow cover that allows greater surface heating and increased soil heat flux.

Modifying the bare soil evaporation and soil thermal conductivity formulations is important for typical early spring conditions with wet soils and sparse green vegetation cover. The bare soil evaporation now falls off more rapidly as the upper layer of the soil dries, with reduced soil heat flux, such that previous excess humidity conditions are abated, and a damped diurnal temperature cycle is ameliorated. Leaf area index and rooting depth changes modestly increase transpiration, reduce sensible heat flux and near-surface air temperature, partially addressing the low-level warm bias in the Eta model during the warm season.

The changes to the Noah LSM described in this study have not completely eliminated Eta model biases thought to be attributable to land-surface processes. As always, several issues remain to be considered in future work: further cold season modifications to the Noah LSM will be necessary to address the remaining cold season bias. The remaining warm season low-level warm bias in the operational Eta model may be related to the underprediction of the plant transpiration by the Noah LSM as noted in offline studies.

The parameterization of surface layer physics should be re-examined to address the uncertainty in surface fluxes and

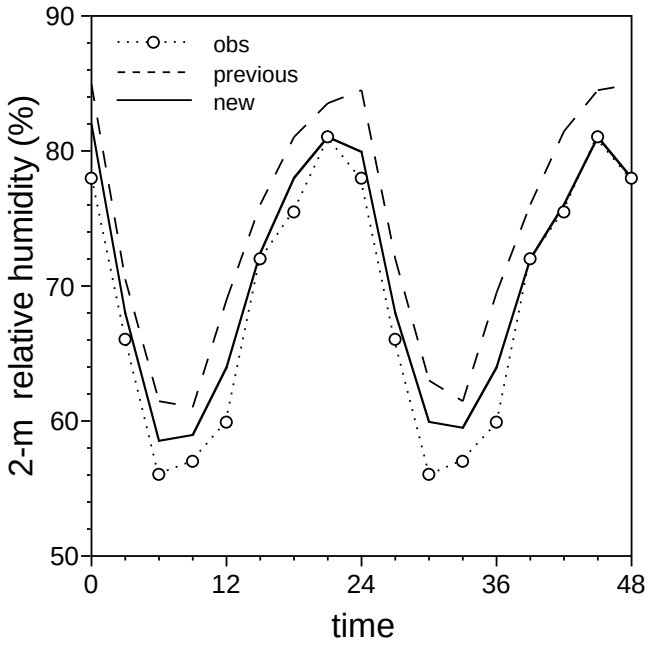

Figure 17. April 2001 monthly composite of 2-m relative humidity, observations (circles-dotted line), and previous (dashed line) and new (solid line) Noah LSM for the US upper midwest (Eta 12Z cycle).

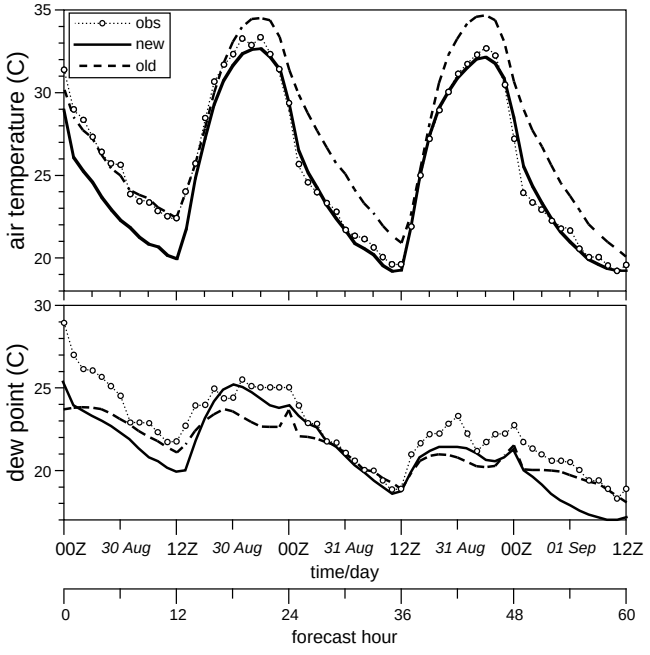

Figure 18. Observed (circles-dotted line) versus modeled 2-m air temperature (upper) and 2-m dew point (lower) for old (dashed lines) and new (solid lines) Noah LSM formulation, at Champaign, Ill. (60-hour Eta model forecast from 00Z 30 August 2000).

the effect on low-level temperatures. Of particular interest is a low-level cold bias that may be due to overly-weak downward sensible heat flux, common under nighttime clear-sky, weak wind conditions especially over snow cover, and a persistent problem in stable boundary layer parameterization. This cold bias may also be affected by the under-forecast of clouds and the associated downward longwave radiation.

Higher resolution surface characteristics, such as soil and land-use classes (e.g. as described in Mitchell et al 2003) and albedo (Csiszar and Gutman 1999) will be tested. Compared to the current vegetation 'climatology' used by the Noah LSM in the Eta model, a realtime weekly green vegetation fraction analysis now operational at NESDIS provides a more realistic surface state, and has shown a positive impact on low-level air temperature forecasts in Eta model tests (Kurkowski et al 2003).

Finally, as a step towards unifying land-surface parameterization at NCEP, plans include testing the Noah LSM in all NCEP/EMC weather and climate models. For example, in addition to the Eta model, the latest operational Noah LSM is currently being used in the NCEP 25-year Regional Reanalysis project (Mesinger et al 2003), tested in the Global Forecast System, and will soon be the default option in the mesoscale Weather Research and Forecasting (WRF) model, to be implemented operationally at NCEP in the future). Such unification allows land-surface states, surface characteristics, and model physics parameters to be more easily and appropriately 'exchanged' between the various modeling systems at NCEP, and elsewhere using the Noah LSM.

Acknowledgments. This research has been supported as the NOAA GCIP Core Project (now GAPP Core Project) through GCIP/GAPP program manager Rick Lawford within the NOAA Office of Global Programs from 1993 to present. Additionally, the cooperation and assistance from Tom Black at the NCEP Environmental Modeling Center, John Schaake and Qingyun Duan at the NWS Office of Hydrologic Development, and Bruce Ramsay at NESDIS/ORA is greatly appreciated. We are also most grateful for the useful comments by two anonymous reviewers. Michael Ek worked on the GCIP Core Project at NCEP under the University Corporation for Atmospheric Research Visiting Scientist Program.

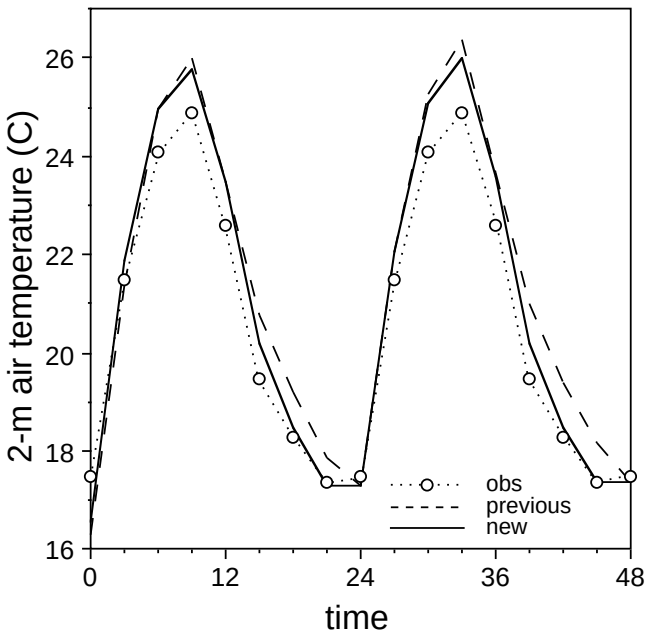

Figure 19. 12 August - 12 September 2000 month-long composite of 2-m air temperature, observations (circles-dotted line), and previous (dashed line) and new (solid line) Noah LSM for the US upper midwest (Eta 12Z cycle).

References

Al Nakshabandi, G. and H. Kohnke, Thermal conductivity and diffusivity of soils as related to moisture tension and other physical properties, *Agric. Meteorol., 2*, 271–279, 1965.

Angevine, W. M., and K. E. Mitchell, Evaluation of the NCEP mesoscale Eta model convective boundary layer for air quality applications, *Mon. Wea. Rev., 129*, 2761–2775, 2001.

Berbery, E. H., Mesoscale moisture analysis of the North American monsoon, *J. Climate, 14*, 121-137, 2001.

Berbery, E. H., Y. Luo, K. E. Mitchell, and A. K. Betts, Eta model-estimated land-surface processes and the hydrologic cycle of the Mississippi basin, *J. Geophys. Res.* (this issue), 2003.

Berbery, E. H., K. E. Mitchell, S. Benjamin, T. Smirnova, H. Ritchie, R. Hogue, and E. Radeva, Assessment of land-surface energy budgets from regional and global models, *J. Geophys. Res., 104 (D16)*, 19,329-19,348, 1999.

Berbery, E. H., E. M. Rasmusson, and K. E. Mitchell, Studies of North American continental-scale hydrology using Eta model forecast products, *J. Geophys. Res., 101 (D3)*, 7305–7319, 1996.

Betts, A. K., F. Chen, K. E. Mitchell, Z. Janjic, Assessment of the land-surface and boundary layer models in the two operational versions of the NCEP Eta model using FIFE data, *J. Geophys. Res., 125*, 2896–2916, 1997.

Black, T., The new NMC mesoscale Eta model: description and forecast examples, *Weather Forecast., 9*, 265–278, 1994.

Boone, A., and P. Etchevers, An inter-comparison of three snow schemes of varying complexity coupled to the same land-surface models: Local scale evaluation at an Alpine site, *J. Hydrometeorol., 2*, 374–394, 2001.

Boone, A., F. Habets, J. Noilhan, The Rhone-AGGregation Experiment, *GEWEX News, WCRP, 11(3)*, 3–5, 2001.

Boone, A., V. Masson, T. Meyers, and J. Noilhan, The influence of the inclusion of soil freezing on simulations by a soil-vegetation-atmosphere transfer scheme, *J. Appl. Meteorol., 39*, 1544–1569, 2000.

Bowling, L. C., D. P. Lettenmaier, B. Nijssen, L. P. Graham, D. B. Clark, M. El Maayar, R. Essery, S. Goers, Y. M. Gusev, F. Habets, B. van den Hurk, J. Jin, D. Kahan, D. Lohmann, X. Ma, S. Mahanama, D. Mocko, O. Nasonova, G.-Y. Niu, P. Samuelsson, A. B. Shmakin, K. Takata, D. Verseghy, P. Viterbo, Y. Xia, Y. Xue and Z.-L. Yang, Simulation of high-latitude hydrological processes in the Torne-Kalix basin: PILPS Phase 2(e) 1: Experiment description and summary intercomparisons, *Global Planet. Change, 38*, 1–30, 2003.

Chang, S., D. Hahn, C.-H. Yang, D. Norquist, and M. Ek, Validation study of the CAPS model land-surface scheme using the 1987 Cabauw/PILPS dataset, *J. Appl. Meteorol., 38*, 405–422, 1999.

Chen, F., Z. Janjic, and K. E. Mitchell, Impact of atmospheric surface-layer parameterizations in the new land-surface scheme of the NCEP mesoscale Eta model, *Bound.-Layer Meteorol., 85*, 391–421, 1997.

Chen, F., and K. E. Mitchell, Using the GEWEX/ISLSCP forcing data to simulate global soil moisture fields and hydrological cycle for 1987-1988, *J. Meteorol. Soc. Japan, 77*, 167–182, 1999.

Chen, F., K. E. Mitchell, J. Schaake, Y. Xue, H.-L. Pan, V. Koren, Q. Y. Duan, M. Ek, and A. Betts, Modeling of land-surface evaporation by four schemes and comparison with FIFE observations, *J. Geophys. Res., 101*, 7251–7268, 1996.

Chen, T. H., A. Henderson-Sellers, P. Milly, A. Pitman, A. Beljaars, F. Abramopoulos, A. Boone, S. Chang, F. Chen, Y.

Dai, C. Desborough, R. Dickinson, L. Duemenil, M. Ek, J. Garratt, N. Gedney, Y. Gusev, J. Kim, R. Koster, E. Kowalczyk, K. Laval, J. Lean, D. Lettenmaier, X. Liang, T.-H. Mengelkamp, J.-F. Mahfouf, K. E. Mitchell, O. Nasonova, J. Noilhan, J. Polcher, A. Robock, C. Rosenzweig, J. Schaake, C. A. Schlosser, J. P. Schulz, Y. Shao, A. Shmakin, D. Verseghy, P. Wetzel, E. Wood, Y. Xue, Z.-L. Yang, and Q.-c. Zeng, Cabauw experimental results from the project for intercomparison of land-surface parameterization schemes (PILPS), *J. Climate, 10*, 1194–1215, 1997.

Csiszar, I., and G. Gutman, Mapping global land surface albedo from NOAA AVHRR, *J. Geophys. Res., 104*, 6215–6228, 1999.

Dorman, J. L, and P. J. Sellers, A global climatology of albedo, roughness length and stomatal resistance for atmospheric general circulation models as represented by the Simple Biosphere model (SiB), *J. Appl. Meteor., 28*, 833–855, 1989.

Gutman, G., and A. Ignatov, The derivation of the green vegetation fraction from NOAA/AVHRR data for use in numerical weather prediction models, *Int. J. Remote Sensing, 19(8)*, 1533–1543, 1998.

Hinkelman, L. M., T. P. Ackerman, and R. T. Marchand, An evaluation of NCEP Eta model predictions of surface energy budget and cloud properties by comparison with measured ARM data, *J. Geophys. Res., 104(D16)*, 19,535–19,549, 1999.

Holtslag, A. A. M., and M. Ek, Simulation of surface fluxes and boundary layer development over the pine forest in HAPEX-MOBILHY, *J. Appl. Meteorol., 35*, 202–213, 1996.

Janjić, Z. I., The step-mountain eta coordinate model: Physical package, *Mon. Wea. Rev., 118*, 1429–1443, 1990.

Janjić, Z. I., The step-mountain eta coordinate model: Further developments of the convection, viscous sublayer, and turbulence closure schemes, *Mon. Wea. Rev., 122*, 927–945, 1994.

Jarvis, P. G., The interpretation of the variations in leaf water potential and stomatal conductance found in canopies in the field, *Phil. Trans. R. Soc. Lond. B., 273*, 593–610, 1976.

Johansen, O., Thermal conductivity of soils (in Norwegian), Ph.D. thesis, Publ. ADA 044002, Trondheim, Norway, 1975. (English translation 637, Cold Reg. Res and Eng. Lab., Hanover, N.H., 1977.)

Kopp, T. J., and R. B. Kiess, The Air Force Global Weather Central snow analysis model, Preprints, 15th Conf. on Weather Analysis and Forecasting, Norfolk, VA, Amer. Meteor. Soc., 220–222, 1996.

Koren, V. , J. C. Schaake, K. E. Mitchell, Q. Y. Duan, F. Chen, and J. Baker, A parameterization of snowpack and frozen ground intended for NCEP weather and climate models, *J. Geophys. Res., 104(D16)*, 19,569–19,585, 1999.

Kurkowski, N. P., D. J. Stensrud, and M. E. Baldwin, Assessment of implementing satellite-derived land cover data in the Eta model, *Wea. Forecast., 18*, 404–416, 2003.

Lunardini, V. J., *Heat Transfer in Cold Climates*, 731 pp., Van Nostrand Reinhold Co., New York, 1981.

Mahfouf, J.-F., and J. Noilhan, Comparative study of various formulations of evaporation from bare soil using in situ data, *J. Appl. Meteorol., 30*, 1354–1365.

Mahrt, L., and M. Ek, The influence of atmospheric stability on potential evaporation, *J. Clim. Appl. Meteorol., 23*, 222–234, 1984

Mahrt, L. and H.-L. Pan, A two-layer model of soil hydrology, *Bound.-Layer Meteorol., 29*, 1–20, 1984.

Marshall, C., Evaluation of the new land-surface and planetary boundary layer parameterization schemes in the NCEP mesoscale Eta model using Oklahoma Mesonet observations, MS thesis, Univ. Oklahoma, School of Meteorol., 176 pp., 1998.

Marshall, C. H., K. C. Crawford, K. E. Mitchell, and D. J. Stensrud, The impact of the land surface physics in the operational NCEP Eta model on simulating the diurnal cycle: Evaluation and testing using Oklahoma Mesonet data, *Wea. Forecast., 18*, 748–768, 2003.

Matthews, E., Global vegetation and land use: New high-resolution data bases for climate studies, *J. Clim. Appl. Meteorol., 22*, 474–487, 1983.

McCumber, M. C. and R. A. Pielke, Simulation of the effects of surface fluxes of heat and moisture in a mesoscale numerical model. Part I: Soil Layer, *J. Geophys. Res., 86*, 9929–9938, 1981.

Mesinger, F., Numerical methods: The Arakawa approach, horizontal grid, global, and limited-area modeling, *General Circulation Model Development: Past, Present and Future*, International Geophysics Series, Vol. 70, D. A. Randall (ed.), Academic Press, 373–419, 2000.

Mesinger, F., G. DiMego, E. Kalnay, P. Shafran, W. Ebisuzaki, Y. Fan, R. Grumbine, W. Higgins, Y. Lin, K. Mitchell, D. Parrish, E. Rogers, W. Shi, D. Stokes, and J. Woolen, NCEP Regional Reanalysis, Symp. on Observing and Understanding the Variability of Water in Weather and Climate, AMS Annual Meeting, Long Beach, CA, February 2003.

Mitchell, K. E., D. Lohmann, P. R. Houser, E. F. Wood, J. C. Schaake, A. Robock, B. A. Cosgrove, J. Sheffield, Q. Duan, L. Luo, R. W. Higgins, R. T. Pinker, J. D. Tarpley, D. P. Lettenmaier , C. H. Marshall, J. K. Entin, M. Pan, W. Shi, V. Koren, J. Meng, B. H. Ramsay, A. A. Bailey, The Multi-institution North American land data assimilation system (NLDAS) project: utilizing multiple GCIP products and partners in a continental distributed hydrological modeling system, *J. Geophys. Res.* (this issue), 2003.

Noilhan, J. and S. Planton, A simple parameterization of land surface processes for meteorological models, *Mon. Wea. Rev., 117*, 536–549, 1989.

Pan, H.-L. and L. Mahrt, Interaction between soil hydrology and boundary-layer development, *Bound.-Layer Meteorol., 38*, 185–202, 1987.

Peters-Lidard, C. D., M. S. Zion and E. F. Wood, A soil-vegetation-atmosphere transfer scheme for modeling spatially variable water and energy balance processes, *J. Geophys. Res., 102(D4)*, 4303–4324, 1997.

Peters-Lidard, C. D., E. Blackburn, X. Liang, and E. F. Wood, The effect of soil thermal conductivity parameterization on surface energy fluxes and temperatures, *J. Atmos. Sci., 55*, 1209–1224, 1998.

Qu, W., A. Henderson-Sellers, A. Pitman, and collaborators, Sensitivity of latent heat flux from PILPS land-surface schemes to perturbations of surface air temperature, *J. Atmos. Sci., 55*, 1909–1927, 1998.

Ramsay, B. H., The interactive multi-sensor snow and ice mapping system, *Hydrological Processes, 12*, 1537-1546, 1998.

Robinson, D. A., and G. Kukla, Maximum surface albedo of seasonally snow covered lands in the Northern Hemisphere, *J. Clim. Appl. Meteorol., 24*, 402–411, 1985.

Rogers, E., T. L. Black, D. G. Deaven, G. J. DiMego, Q. Zhao, M. Baldwin, N. Junker, and Y. Lin, Changes to the operational 'early' Eta Analysis/Forecast System at the National Centers for Environmental Prediction, *Weather Forecast., 11*, 391–413, 1996.

Schaake, J. C., V. I. Koren, Q.-Y. Duan, K. E. Mitchell, and F. Chen, Simple water balance model for estimating runoff at different spatial and temporal scales, *J. Geophys. Res., 101*, 7461-7475, 1996.

Schlosser, C. A., A. G. Slater, A. Robock, A. J. Pitman, K. Y. Vinnikov, A. Henderson-Sellers, N. A. Speranskaya, K. E. Mitchell, A. Boone, H. Braden, F. Chen, P. Cox, P. de Rosnay, C. E. Desborough, R. E. Dickinson, Y.-J. Dai, Q. Duan, J. Entin, P. Etchevers, N. Gedney, Y. M. Gusev, F. Habets, J. Kim, V. Koren, E. Kowalczyk, O. N. Nasonova, J. Noilhan, J. Schaake, A. B. Shmakin, T. G. Smirnova, D. Verseghy, P. Wetzel, Y. Xue, and Z.-L. Yang, Simulations of a boreal grassland hydrology at Valdai, Russia: PILPS Phase 2(d), *J. Geophys. Res., 128*, 301-321, 2000.

Sellers, P. J., B. W. Meeson, J. Closs, J. Collatz, F. Corprew, D. Dazlich, F. G. Hall, Y. Kerr, R. Koster, S. Los, K. Mitchell, J. McManus, D. Myers, K.-J. Sun, and P. Try, An overview of the ISLSCP initiative i global data sets, on: ISLSCP Initiative I - Global Data Sets for Land-Atmosphere Models, 1987-1988, Volumes 1-5, published on CD by NASA, volume 1: USA_NASA_GDAAC_ISLSCP_001, OVERVIEW.DOC, 1995.

Slater, A. G., C. A. Schlosser, C. E. Desborough, A. J. Pitman, A. Henderson-Sellers, A. Robock, K. Ya. Vinnikov, K. E. Mitchell, A. Boone, H. Braden, F. Chen, P. M. Cox, P. de Rosnay, R. E. Dickinson, Y.-J. Dai, Q. Duan, J. Entin, P. Etchevers, N. Gedney, Ye. M. Gusev, F. Habets, J. Kim, V. Koren, E. A. Kowalczyk, O. N. Nasonova, J. Noilhan, S. Schaake, A. B. Shmakin, T. G. Smirnova, D. Verseghy, P. Wetzel, Y. Xue, Z.-L. Yang, Q. Zeng, The representation of snow in land surface schemes: results from PILPS 2(d), *J. Hydrometeor., 2*, 7–25, 2001.

Smirnova, T. G., J. M. Brown, S. G. Benjamin, and D. Kim, Parameterization of cold-season processes in the MAPS land-surface scheme, *J. Geophys. Res., 105*, 4077–4086, 2000.

van den Hurk, B. J. J. M., P. Viterbo, A. C. M. Beljaars, and A. K. Betts, Offline validation of the ERA40 surface scheme, ECMWF Tech. Mem. 295, 42 pp, 2000.

Viterbo, P., A. Beljaars, J.-F. Mahfouf, and J. Teixeira, The representation of soil moisture freezing and its impact on the stable boundary layer, *Quart. J. Roy. Meteorol. Soc., 125*, 2401–2426, 1999.

Wood, E. F., D. P. Lettenmaier, X. Liang, D. Lohmann, A. Boone, S. Chang, F. Chen, Y. Dai, R. E. Dickinson, Q. Duan, M. Ek, Y. M. Gusev, F. Habets, P. Irannejad, R. Koster, K. E. Mitchell, O. N. Nasonova, J. Noilhan, J. Schaake, A. Schlosser, Y. Shao, A. B. Shmakin, D. Verseghy, K. Warrach, P. Wetzel, Y. Xue, Z.-L. Yang, Q.-c. Zeng, The project for intercomparison of land-surface parameterization schemes (PILPS) phase 2(c) Red–Arkansas river basin experiment: 1. Experiment description and summary intercomparisons, *Global Planet. Change, 19*, 115-135, 1998.

Yang, Z.-L., Y. Dai, R. E. Dickinson, and W. J. Shuttleworth, Sensitivity of ground heat flux to vegetation cover fraction and leaf area index, *J. Geophys. Res., 104(D16)*, 19,505–19,514, 1999.

Yucel, I., W. J. Shuttleworth, J. Washburne, and F. Chen, Evaluating NCEP Eta model derived data against observations, *Mon. Wea. Rev., 126*, 1977–1991, 1998.

Michael B. EK, NOAA Science Center, NCEP/EMC, 5200 Auth Rd, Rm 207, Suitland, MD 20746-4304 USA. michael.ek@noaa.gov

(Received _____.)